THE ASTROPHYSICAL JOURNAL, 437:L123–L125, 1994 December 20

GASDYNAMICAL APPROACH TO A FACE-ON VIEW OF THE MILKY WAY

KEIICHI WADA
Center for Information Processing Education, Hokkaido University, Sapporo 060, Japan
YOSHIAKI TANIGUCHI
Astronomical Institute, Tohoku University, Sendai 980-77, Japan
ASAO HABE
Department of Physics, Hokkaido University, Sapporo 060, Japan
AND
TETSUO HASEGAWA
Institute of Astronomy, The University of Tokyo, Mitaka, Tokyo 181, Japan
Received 1994 July 19; accepted 1994 October 6

ABSTRACT

Analyses of the distribution of far-infrared point sources in the Galactic bulge have suggested that from a face-on perspective the bulge has a barlike shape. Here, we investigated how a rotating barlike bulge affects the global gasdynamics in a disk and compare the longitude-velocity (LV) maps from self-gravitating hydrodynamical simulations with observed maps of neutral hydrogen and carbon monoxide in the Galaxy. We found that the features on the numerical LV maps depend strongly on four factors: the pattern speed of the bar, the position angle of the Sun, the strength of the bar potential, and the ratio of the gas mass to total dynamical mass. We conclude that our Galaxy has a rotating, weak, barlike bulge observed from nearly end-on. The allowed range of pattern speed of the bar is surprisingly narrow and is consistent with recent observations of bulge stars. Self-gravity of the interstellar matter is needed to account for some of the observations.

Subject headings: Galaxy: structure — ISM: kinematics and dynamics — methods: numerical

1. INTRODUCTION

In order to deduce the face-on appearance of the Milky Way (MW), a number of studies have been made using both longitude-velocity (LV) diagrams of the CO and H I emission lines (e.g., Burton 1985; Dame et al. 1987) and rotation curves derived from the gas motion (Burton & Gordon 1978; Clemens 1985). Provided that the gravitational potential of our Galaxy is axisymmetric, the LV diagrams and the rotation curves tell us the distribution of the interstellar matter as well as the gravitational potential. However, LV diagrams include evidence for noncircular gas motion, and a pronounced maximum at 1 kpc and a dip at 3 kpc in the rotation curve are likely to arise from nonaxisymmetry in the gravitational potential of our Galaxy (Combes 1991). Moreover, some direct photometric lines of evidence and theoretical studies have suggested that the central bulge of the MW is a stellar bar (Blitz et al. 1993).

In previous theoretical studies elliptical stellar orbits in a barred potential have often been used to explain the observed noncircular gas motion (Simonson & Mader 1973; Peters 1975; Manabe & Miyamoto 1975; Blitz & Spergel 1991a). However, while this approach may be useful for describing the dynamics of the molecular gas in the central part of our Galaxy (Binney et al. 1991), it is not adequate on a global scale because the gas responds sensitively and nonlinearly to even weak distortions in the gravitational potential (Wada 1994). The effect of self-gravity of the gaseous component on its own dynamics, especially in a barred potential, is also significant and must be incorporated into the study.

A previous hydrodynamical treatment assumed that the bar extends to the radius of the outer Lindblad resonance (Mulder & Liem 1986). However, many recent observations have suggested the presence of a more compact bar in our Galaxy (Nakada et al. 1991; Weinberg 1992; Blitz & Spergel 1991b). In this *Letter*, we verify the bar hypothesis of our Galaxy by two-dimensional fully time-dependent numerical simulations with a self-gravitating smoothed particle hydrodynamics (SPH) code and analysis of the resulting numerical LV diagrams.

2. MODELS AND METHOD

The gravitational potential is assumed to have the form $\Phi(R, \theta) = \Phi_0(R)[1 + \Phi_b(R) \cos 2\theta]$ with axisymmetric part $\Phi_0(R) = -\sqrt{27/4}\, a v_{\max}^2/\sqrt{R^2 + a^2}$; $v_{\max}$ is the maximum circular velocity, and a is a core radius (Toomre 1963; Matsuda & Isaka 1980). This form of the potential is a good approximation for the inner part of disk galaxies. We set $v_{\max} = 250$ km s^{-1} and $a = 2$ kpc. (We also examined models with a larger core size [$a = 4$ kpc], although this bulge is not as compact as the one observed by *COBE*. We found that the observed gaseous features of the Galactic LV diagrams cannot be reproduced in these models.) The amplitude of the nonaxisymmetric distortion of the potential is taken to be $\Phi_b(R) = \epsilon a R^2/(R^2 + a^2)^{1.5}$, where ϵ is a parameter which represents the strength of the bar potential (Sanders 1977). This potential implies a weakly distorted mass distribution of a size approximately a and is a model of a galaxy with a compact and weak bar. We have explored models with $\epsilon = 0.05$, 0.1, and 0.2. Axial ratios of the bulge implied by the potential are 0.9, 0.7, and 0.5, respectively.

An SPH scheme and particle-mesh algorithm with FFT for calculating self-gravity are used to simulate the gas response in an infinitesimally thin disk (Wada & Habe 1992). The gas is isothermal and initially is uniformly distributed in a disk of radius 8 kpc. The ratio of the gas mass ($3.8 \times 10^9\ M_\odot$) in the initial uniform disk to the background dynamical mass within

TABLE 1

MODEL PARAMETERS

Model	Ω_b[a]	a/b[b]	f[c]
A	60	0.7	0.05
B	24	0.7	0.05
C	19	0.7	0.05
D	19	0.7	0.00
E	14	0.7	0.05
F	24	0.5	0.05
G	19	0.5	0.05
H	19	0.9	0.05

[a] Pattern speed of the barlike bulge (km s^{-1} kpc^{-1}); $v_{LSR} = 220$ km s^{-1} and $R_{LSR} = 8.5$ kpc are assumed.
[b] Axial ratio of the barlike bulge.
[c] Fraction of gas mass to the dynamical mass inside the LSR at initial. Zero means a run without self-gravity of the gas.

8 kpc is 5%. In a quasi–steady state the total mass of SPH particles inside 8.5 kpc is $3.2 \times 10^9\ M_\odot$. Our models are summarized in Table 1.

3. THE PATTERN SPEED AND THE POSITION ANGLE OF THE BAR

There are two prominent features in the observed H I and CO LV diagrams (e.g., Burton 1985; Dame et al. 1987). One is the high-velocity component near the Galactic center, sometimes called the nuclear disk. The other is a molecular ring observed in the range of $l \simeq 330°$–$30°$ (Dame 1987). Any theoretical models should explain these features. In the following, we devote our attention to these two prominent observational features and compare them with our numerical results.

First, we consider the origin of the nulcear high-velocity component observed both in H I and in CO. In order to explain this component within the framework of an axisymmetric potential, it is necessary to postulate the presence of a massive component at the center ($\sim 10^{10}\ M_\odot$) and an outward radial motion of ~ 70 km s^{-1}. However, if the gaseous orbits are elongated, we are able to explain the high-velocity nuclear component without any expanding or infalling motions or the hypothetical massive nucleus. If the line of sight is nearly parallel to the major axis of the elliptical streamlines, the apparent velocity of the gas near the Galactic center changes rapidly depending on the viewing angle (Binney et al. 1991).

In Figure 1 (Plate L10) we show the quasi–steady state gas distribution of model C. This has a barlike bulge with axial ratio = 0.7 and a pattern speed of $\Omega_b = 19$ km s^{-1} kpc^{-1}, which is $\simeq \frac{2}{3}$ the maximum of $(\Omega_0 - \kappa_0/2)$, where Ω_0 and κ_0 are the circular and the epicyclic frequency, respectively. We assume here that the rotation velocity of the local standard of rest is $v_{LSR} = 220$ km s^{-1} and the Galactocentric radius of the Sun is $R_\odot = 8.5$ kpc. In Figure 1*a* we can see three prominent features: (1) a central elongated gas component with very high density, (2) a dense oval ring around 4 kpc from the center, and (3) two weak spiral arms starting at the ring. The first feature begins as two leading, poor spiral arms formed near the *inner* inner Lindblad resonance (ILR), and it is stable because the ratio of gas mass to background mass (0.05 in the present model) is less than the critical value for gravitational instability (Fukunaga & Tosa 1991; Wada & Habe 1992). The second and the third features are evolved from the two trailing spiral arms that formed near the *outer* ILR (Wada 1994).

The central elongated gas component is a product of the very weak nonaxisymmetrical potential. The streaming of the gas in this region is shown in Figure 1*b*. In Figure 2 (Plate L11) we present the theoretical LV diagrams derived from the steady state gas distribution given in Figure 1*a*. Figures 2*a* and 2*b* correspond to observations from azimuthal angles, 10° and 90°, respectively, measured counterclockwise with respect to the major axis of the bar. If we observe the nuclear region of the simulations from along the minor axis of the barlike bulge, the gas ring appears as a dense feature with $|l| < 10°$ on the LV diagram, but it does not have any high-velocity components. On the other hand, if we observe this elongated gas component nearly from the end on, we can successfully explain the observed high-velocity gas component in the LV diagrams. An LV diagram for the position angle 30° (Fig. 2*c*) shows that the central high-velocity component has a width of about 10°, whereas an observed one is about 5°. We have calculated LV diagrams for position angle between 90° and −90° and conclude that the position angle of the LSR must be less than 20° from the major axis of the barlike bulge.

CO surveys of the MW have revealed that much molecular gas is concentrated in a ring, peaking at 4–5 kpc from the Galactic center (Scoville & Solomon 1975; Gordon & Burton 1976; Robinson et al. 1984; Bronfman et al. 1988), which is seen in the range $330° < l < 30°$ on the LV diagrams. Further, there is a very strong concentration of molecular gas around the Galactic center where its surface density is at least 10 times larger than that in the molecular ring (Bania 1977; Liszt & Burton 1978; Combes 1991). Figure 3 shows the radial distribution of the gas surface density for each model. The observed gaseous concentrations both at around 4 kpc and at the center (see, e.g., Nakai 1992) are reproduced only in Model C. Moreover, the pronounced maximum and dip in the observed rotation curves obtained using terminal velocity information from the H I and CO emission data (Burton & Gordon 1978; Clemens 1985) can naturally be explained from the theoretical LV diagram (Fig. 2*a*). These features in the rotation curves are due to noncircular motion of the gas. In short, our hydrodynamical model can reproduce the apparent distribution and kinematics of gas simultaneously for a specific set of parameters.

In the above simulation, we took the pattern speed to be $\Omega_b = 19$ km s^{-1} kpc^{-1}. A value close to this is needed in order

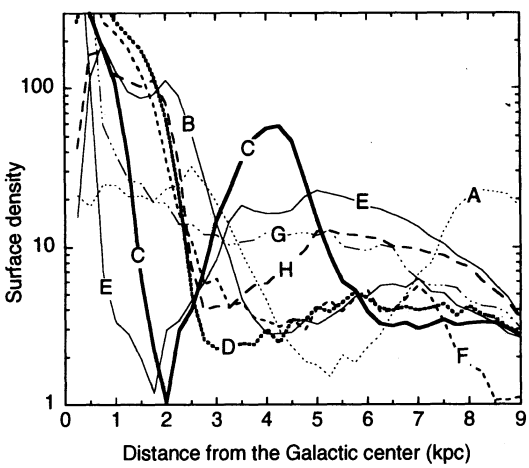

FIG. 3.—Radial surface density distributions of the gas of model A–H. Unit of the vertical axis is $M_\odot$ pc^{-2}.

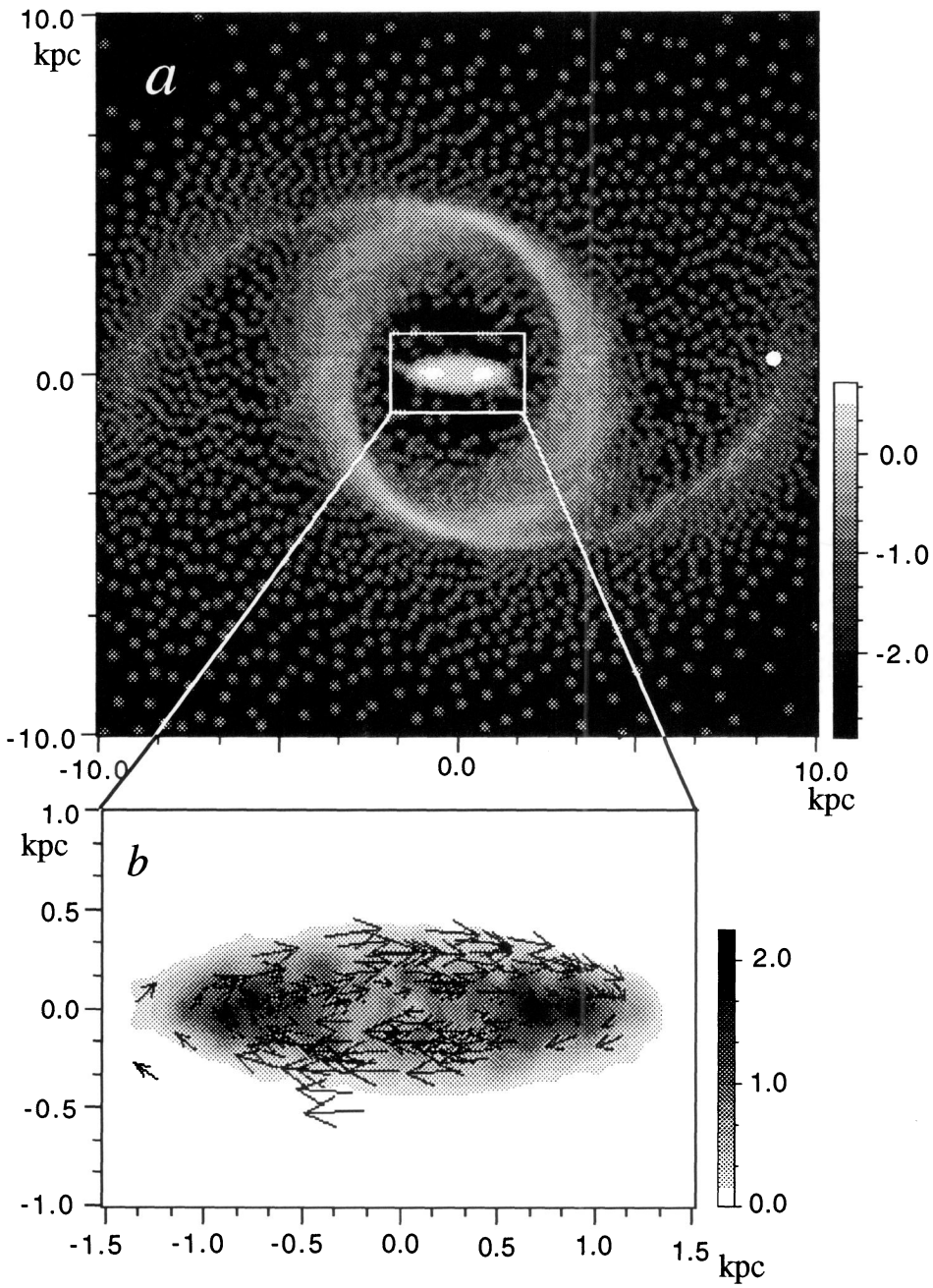

FIG. 1.—(*a*) Gas density distribution of a self-gravitating model with $\Omega_b = \frac{2}{3}$ max $(\Omega_0 - \kappa_0/2)$ in the model with $\epsilon = 0.1$ (model C) in a quasi–steady state. The ILRs are located at 1 and 6 kpc from the center. The major axis of the bar is parallel to the x-axis of the figure. Gases rotate clockwise. The gray scale represents surface density, $\log_{10}(\Sigma/\Sigma_0)$, with $\Sigma_0 \equiv 1.5 \times 10^2\ M_\odot\ \mathrm{pc}^{-2}$. The most probable position of the LSR is shown by a white filled circle. (*b*) A close-up of the nuclear disk in (*a*). Velocity vectors of the gases are also shown. The maximum length of the arrows is about 200 km s^{-1}. The gray scale represents surface density, Σ/Σ_0, $\Sigma_0 \equiv 1.5 \times 10^2\ M_\odot\ \mathrm{pc}^{-2}$.

WADA et al. (see 437, L124)

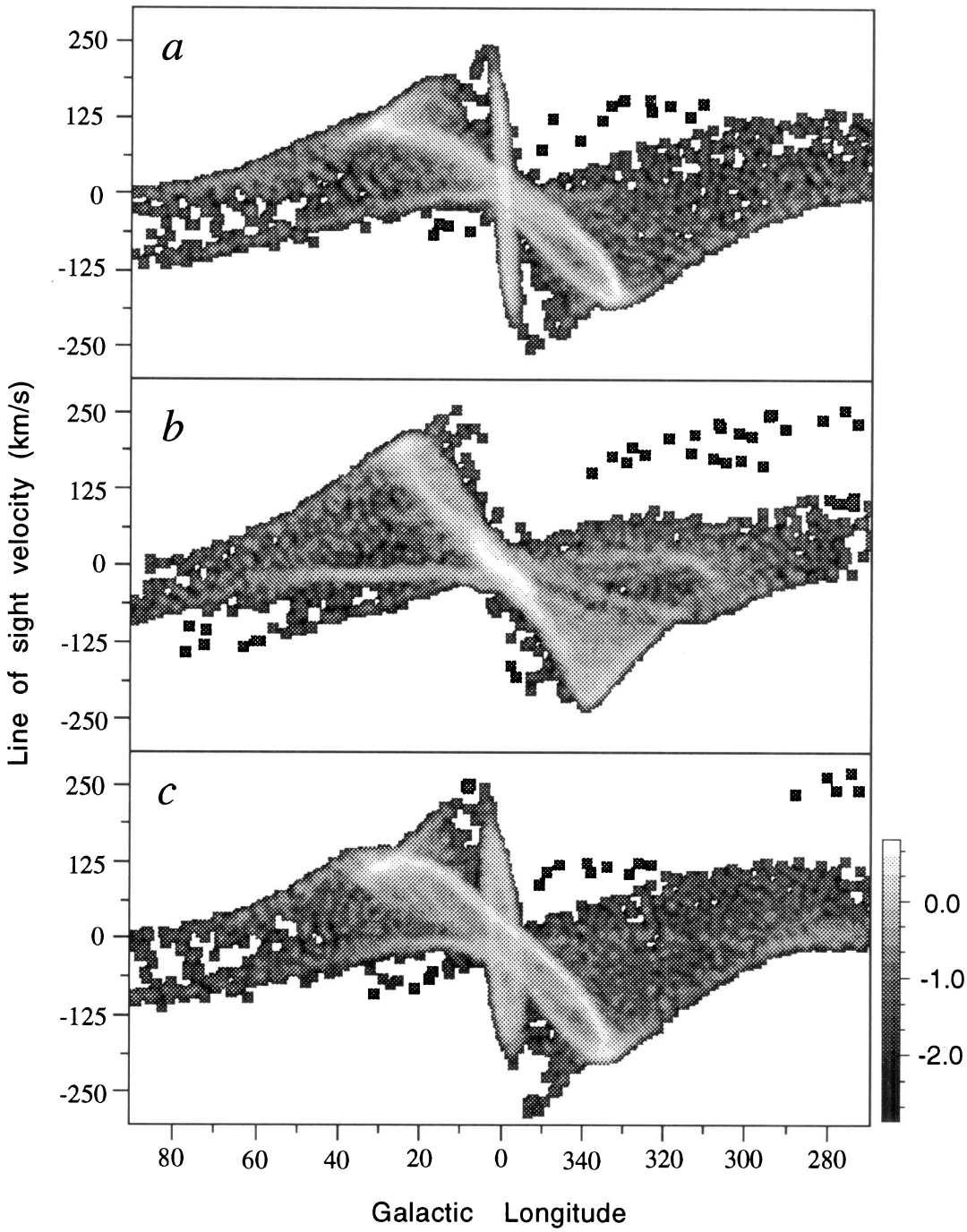

FIG. 2.—(*a*) Longitude-velocity diagram for Fig. 1*a*. The position angle of the LSR, θ_p, is 10°, measured counterblockwise from the major axis of the bar. The vertical axis is velocity, and the horizontal axis is Galactic longitude. The gray scale represents surface density on the LV plane, $\log_{10}(\mu/\mu_0)$, $\mu_0 \equiv 3 \times 10^5$ $M_\odot$/(km s^{-1} deg). (*b*) Same as (*a*), but for $\theta_p = 90°$. (*c*) Same as (*a*), but for $\theta_p = 30°$.

to reproduce the observed nuclear high-velocity component. If we take the case of a slowly rotating bar (model E: $\Omega_b = 14$ km s^{-1} kpc^{-1}), the gas distribution in a quasi-steady state shows two trailing spiral arms with small pitch angles, associated with a hole inside the second ILR, and a central dense core with small size. In this case, no high-velocity component in the center can be seen at any position angle on the LV diagram. This result is shown in Figure 4*b* (Plate L12). On the other hand, for larger $\Omega_b = 24$ km s^{-1} kpc^{-1} (model B), although a nuclear disk is formed, there is no dense "molecular ring" structure on the LV diagram in a quasi-steady state (Fig. 4*a*). In much faster bar model (model A) in which there are no ILRs, the nuclear disk is not formed. Surprisingly, the range of allowed Ω_b is quite narrow.

Furthermore, we note that the pattern speed of the bar, 19 km s^{-1} kpc^{-1}, is consistent with a recent observation of the bulge stars. Nakada et al. (1993) obtained a mean rotational velocity of 9 km^{-1} deg^{-1} = 60 km s^{-1} kpc^{-1} for OH-IR stars in the Galactic bulge. Previous *N*-body simulations have shown that the mean orbital velocity of the stars in a bar is 2 or 3 times larger than the pattern velocity of the bar, if the viewing angle is along the bar (Sellwood 1981).

4. SELF-GRAVITY OF THE GAS AND THE STRENGTH OF THE BAR

Another very important point is the effect of self-gravity of gas even if the gas mass fraction is small (e.g., 5%). We have run a simulation without the self-gravity of gas (model D), but with the other parameters the same as in model C. In this case, the gas starts to accumulate in a molecular ring, but this ring does not grow and finally becomes a very weak structure. Hence, we cannot reproduce the observed LV diagrams at all, as is shown by Figure 4. Therefore, the effect of the self-gravity of the gas is absolutely necessary to reproduce the molecular ring at a radius of 4 kpc. In our model of the Galaxy, the total mass of the gas is $3.2 \times 10^9\ M_\odot$ in 8.5 kpc in the quasi–steady state, whereas observations suggest that the total mass of H_2 inside the solar radius is $2–3 \times 10^9\ M_\odot$ (Combes 1991).

Finally, we mention an important constraint about the strength of the bar. We have tried to reproduce the observed LV diagrams with a more strongly distorted barlike potential. However, even in the case of $a/b = 0.5$ in the mass distribution (models F and G), we cannot reproduce the observed LV diagram for any position angle at all. Thus, we conclude that the bar cannot be very strong. But a weaker bar with $a/b = 0.9$ (model H) also fails to produce any molecular ring (see Fig. 3).

5. CONCLUSION

Hydrodynamical approaches turn out to be very useful for determining the structure of galaxies. We conclude that the bulge of our Galaxy has a weak barlike shape with an axial ratio of about 0.7. This weak bar rotates with an angular pattern speed of $19 \pm 5\ (v_{\rm LSR}/220\ {\rm km\ s^{-1}})(R_\odot/8.5\ {\rm kpc})^{-1}$. The line of sight makes an angle of less than 20° with the major axis of the bar. The distorted bulge enhances the observed nonuniform and nonaxisymmetric distribution in the self-gravitating interstellar gas in our Galaxy.

We can also apply the presented method to the studies of external edge-on galaxies. For example, the well-studied nearby edge-on disk galaxy NGC 891 also has a central high-velocity component and a molecular ring on its observed H I and CO position-velocity diagrams (Sofue & Nakai 1993). The present study suggests that NGC 891 is quite similar to our Galaxy not only from the edge-on view, but also the face-on view. Note that our Galaxy and NGC 891 are not necessarily "barred" galaxies but are ordinary spiral galaxies classified as Sb ~ Sc in the classification scheme of Hubble. Our Galaxy and NGC 891 should look like NGC 309 (Sc), which has a weakly distorted bar with two open spiral arms in the infrared light but shows very rich star-forming regions in the disk (Block & Wainscoat 1991).

We thank Y. Sofue and D. Walsh for their fruitful suggestions. This work were partially supported by a grant from the Institute of Space and Astronautical Science, Japan, and Nukazawa Science Foundation.

REFERENCES

Bania, T. M. 1977, ApJ, 216, 381
Binney, J. J., Gerhard, O. E., Stark, A. A., Bally, J., & Uchida, K. I. 1991, MNRAS, 252, 210
Blitz, L., Binney, J., Lo, K. Y., Bally, J., & Ho, P. T. P. 1993, Nature, 361, 417
Blitz, L., & Spergel, D. N. 1991a, ApJ, 370, 205
———. 1991b, ApJ, 379, 631
Block, D. L., & Wainscoat, R. J. 1991, Nature, 353, 48
Bronfman, L., Cohen, R. S., Alvarez, H., May, J., & Thaddeus, P. 1988, ApJ, 324, 248
Burton, W. B. 1985, A&AS, 62, 365
Burton, W. B., & Gordon, M. A. 1978, A&A, 63, 7
Clemens, D. P. 1985, ApJ, 295, 422
Combes, F. 1991, ARA&A, 29, 195
Dame, T. M., et al. 1987, ApJ, 322, 706
Fukunaga, M., & Tosa, M. 1991, PASJ, 43, 469
Gordon, M. A., & Burton, W. B. 1976, ApJ, 208, 346
Liszt, H. S., & Burton, W. B. 1978, ApJ, 226, 790
Manabe, S., & Miyamoto, M. 1975, PASJ, 27, 35
Matsuda, T., & Isaka, H. 1980, Prog. Thoer. Phys., 64, 1265
Mulder, W. A., & Liem, B. T. 1986, A&A, 157, 148
Nakada, Y., Deguchi, S., Hashimoto, O., Izumiura, H., Onaka, T., Sekiguchi, K., & Yamamura, I. 1991, Nature, 353, 140
Nakada, Y., Onaka, T., Yamamura, I., Deguchi, S., Ukita, N., & Izumiura, H. 1993, PASJ, 45, 179
Nakai, N. 1992, PASJ, 44, L27
Peters, W. L. 1975, ApJ, 195, 617
Robinson, B. J., Manchester, R. N., Whiteoak, J. B., Sanders, D. B., Scoville, N. Z., Clemens, D. P., McCutecheon, W. H., & Solomon, P. M. 1984, ApJ, 283, L31
Sanders, R. H. 1977, ApJ, 217, 916
Scoville, N. Z., & Solomon, P. M. 1975, ApJ, 199, L105
Sellwood, J. A. 1981, A&A, 99, 362
Simonson, S. C., & Mader, G. L. 1973, A&A, 27, 337
Sofue, Y., & Nakai, N. 1993, PASJ, 45, 139
Toomre, A. 1963, ApJ, 138, 386
Wada, K. 1994, PASJ, 46, 165
Wada, K., & Habe, A. 1992, MNRAS, 258, 82
Weinberg, M. D. 1992, ApJ, 384, 81

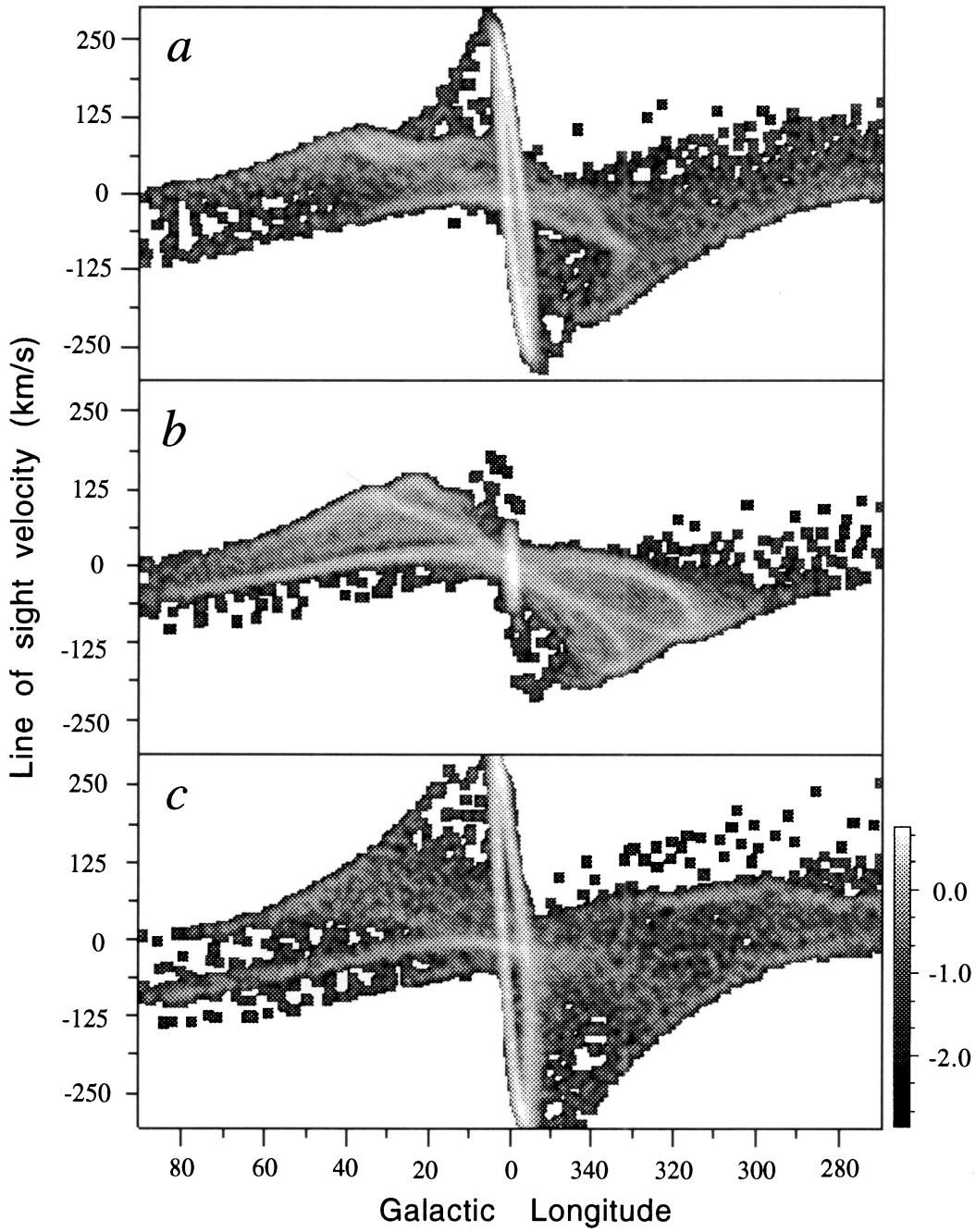

FIG. 4.—(*a*) Same as Fig. 2*a*, but for faster pattern speed model (model B). (*b*) Same as Fig. 2*a*, but for slower pattern speed model (model E). (*c*) Same as Fig. 2*a*, but for non–self-gravitating model (model D).